DOI 10.1007/s11182-024-03139-8
Russian Physics Journal, Vol. 67, No. 4, April, 2024

PRODUCTION OF EXPERIMENTAL SAMPLES OF NICKEL-BASED ALLOY AND COPPER NOZZLES BY ELECTRON BEAM ADDITIVE MANUFACTURING

Y. V. Kushnarev, V. M. Semenchuk, A. V. Chumaevskii, K. S. Osipovich, V. E. Rubtsov, and E. A. Kolubaev

UDC 620.184.3

In this work, the characteristics of surface morphology and structure of experimental samples of nickel-based alloy and copper nozzles manufactured by the electron beam additive method have been studied. It is found that the grain boundaries on the outer sample surface are oriented at different angles relative to the substrate due to uneven heat dissipation during printing. It is found that 3D printing in a non-optimal temperature regime produces a highly heterogeneous structure within the material layer. A curvilinear boundary zone is observed in which different structural phase components are formed, including solid solutions and mechanical mixtures.

Keywords: electron beam additive manufacturing, nickel alloy, copper, microstructure, microsegregation.

INTRODUCTION

Additive manufacturing of complex 3D parts from heterogeneous materials is of great technical interest because it enables parts to be used in a variety of applications where two criteria should be met simultaneously, namely, light weight and thermal conductivity, or heat resistance and electrical conductivity [1]. The main materials used in the aerospace industry are aluminum alloys, stainless steels, titanium alloys, nickel and iron-based superalloys, copper, cobalt, and refractory alloys, and some other materials. Currently, more than 50% of the mass of a modern aircraft engine is manufactured from high-temperature nickel-based superalloys [2]. The nickel alloys are used for casting blades and other components of advanced gas turbine engines operating at high temperatures in aviation and electrical power generation industries [2]. Their excellent mechanical properties at extremely high temperatures and pressures in aggressive environments significantly increase the efficiency of modern aircraft engines [3]. Despite excellent mechanical properties of the nickel alloy, its limited thermophysical properties do not allow its use under conditions of intensive heat dissipation (e.g. in combustion chambers and nozzles [4]). Typically, a cooling channel is designed between the nickel alloy and a material with high thermal conductivity such as copper. The copper alloys are commonly used in heat exchangers such as combustion chambers of liquid rocket engines. This high heat flux environment requires an alloy with high strength and thermal conductivity to properly cool the walls of the thrust chamber with fuel or high-pressure oxidizer [5, 6]. Our literature analysis showed wide practical application of such compounds for manufacture of the combustion chambers using GRCop-42 and C18150 copper alloys, Inconel 718 nickel superalloys, and their bimetallic compounds; channel-cooled nozzles using JBK-75, NASA HR-1, Inconel 625, and Haynes 230 alloys; and bimetallic structures using copper-nickel superalloys [7, 8]. Despite the fact that Cu and Ni are fully miscible and have the same FCC crystal structures and close densities (8.93 g/cm^3 for Cu and 8.88 g/cm^3 for Ni), these materials are difficult to co-print by the additive manufacturing technique. For example, the mismatch in thermal conductivities (398 W/mK for Cu and 60.7 W/mK for Ni), melting points (1356 K for Cu and 1728 K for Ni), thermal expansion coefficients ($16.4 \cdot 10^6$ K^{-1} for Cu and $13.1 \cdot 10^6$ K^{-1} for Ni), and Young's moduli (130 GPa for Cu and

Institute of Strength Physics and Materials Science of the Siberian Branch of the Russian Academy of Sciences, Tomsk, Russia, e-mail: tch7av@gmail.com. Original article submitted December 20, 2023.

TABLE 1. Chemical Compositions of the Steel Substrates and Wires Used in the Work

Material	Chemical element (wt.%)									
	Fe	Cu	Ni	Cr	Mo	Nb	Mn	Si	Cu	C
AISI 321	~67	–	8–9.5	17–19	–	–	<2	<0.8	<0.3	<0.12
Inconel 625	<5.0	–	>58.0	20–23	8–10	3.15–4.15	<0.5			<0.1
Pure copper	<0.005	99.9	<0.002	–	–		–	–	–	–

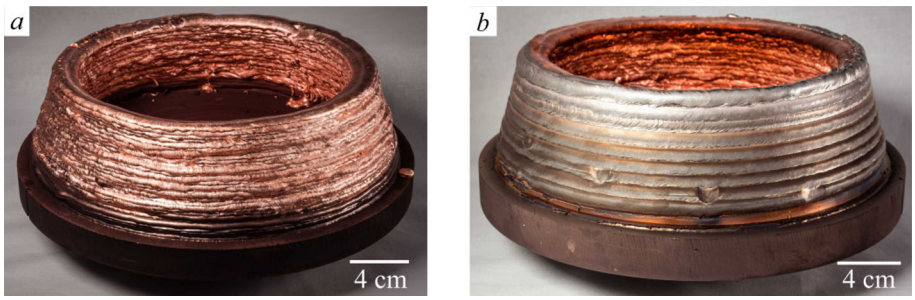

Fig. 1. General view of the EBAM formed sample: the copper cone (*a*) and the subsequent nickel layers (*b*).

110 GPa for Ni) creates significant thermal stresses when laser powder bed deposition technique is used [2]. Changing the process parameters and scanning strategy affects the process and therefore the quality and properties of the manufactured parts [1]. As a result, multi-material 3D products that can be produced using current additive manufacturing techniques are still limited in terms of possible geometries and material combinations. In addition, no systematic attempt has been made to find the conditions for combining heterogeneous materials into complex geometries. The purpose of the present work is to investigate the structure and properties of experimental samples of nickel alloy and copper nozzles manufactured by the electron-beam additive method under different conditions. The present research makes a significant contribution to the development of theory of structure formation in polymetallic materials produced by additive manufacturing. The results obtained can be used to select and specify the parameters and structural states of materials with specified properties that provide the necessary force and temperature modes of device operation.

MATERIALS AND METHODS

The samples were fabricated at the ISPMS SB RAS on the experimental equipment for electron beam additive manufacturing. To produce the nozzle samples, stainless steel SS321 substrates of different thickness and wires made of copper and nickel alloy Inconel 625 with a diameter of 1.2 mm were used (Table 1).

The main manufacturing parameters in this case were the acceleration voltage and the electron beam current. It was found that the electron beam current, the thickness of the employed substrate, and the size of the experimental sample to be formed influenced significantly. On this basis, samples of two types were analyzed to produce defect-free samples of complex geometry. In the first printing mode, a thin substrate with thickness of 0.5 cm and a smaller geometric nozzle size (with a diameter of 25 cm and a height of 6 cm) was chosen; in the second printing mode, a thick substrate with thickness of 2 cm and a larger geometric nozzle size (with a diameter of 13.5 cm and a height of 9 cm) was chosen. Since the electron beam current varied during 3D printing with heterogeneous materials, its variation for the whole product was evaluated by the heat input: it was smaller in the first case than in the second case. At the beginning, two layers of pure copper were grown on the substrate to form a cone (Fig. 1*a*). Then the resulting surface was prepared by mechanical treatment. After that, the 3D printing direction was changed by 90° relative to the

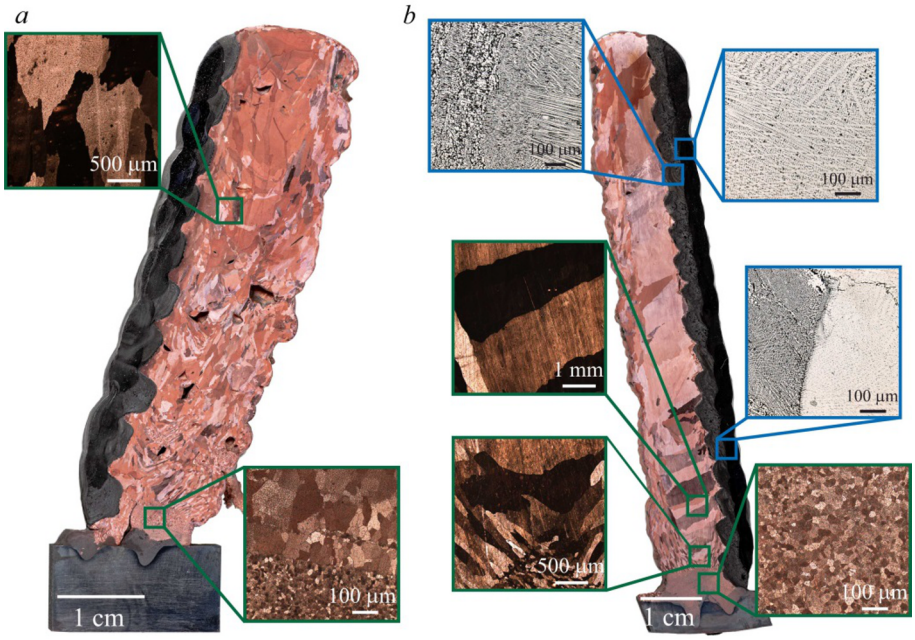

Fig. 2. Cross sections of the samples with enlarged optical microscopy images of the experimental nozzles based on nickel alloy and copper of the nozzles of the first (*a*) and second types (*b*).

substrate. In this position, the printing of two nickel alloy layers was continued (Fig. 1*b*). The nickel layers had a thickness of about 2–3 mm with an overlap of 1 mm and did not show the formation of defects.

To study the macro- and microstructure of the grown experimental nozzle models, specimens were cut using a DK7750 electric discharge machine. To study the macrostructure, flat samples were cut in cross section. Prior to the structural studies, the samples were ground and polished by the standard method, and their polished surfaces were then etched at 80°C for 15 min in a solution of 8 g $CuSO_4$ + 40 ml C_2H_5OH + 40 ml HCl. The macroscopic images of the specimens were taken with the Pentax K-3 camera equipped with the lens having a focal length of 100 mm. Optical studies were performed using an OLYMPUSLEXT confocal microscope (Olympus NDT Inc., Waltham, the USA). A portable Niton XL3T spectrometer was used to determine the elemental composition of the samples. Tensile specimens with working part size of 12 × 2.0 × 2.7 mm^3 cut in cross-section from the bottom, center, and top of the experimental nozzle were used to study their mechanical characteristics. Mechanical tests were performed on a universal testing machine UTS 110M with a strain rate of $1.4 \cdot 10^{-3}$ s^{-1}.

RESULTS AND DISCUSSION

The cross sections of the samples grown by electron beam additive manufacturing using filaments of dissimilar materials of Udimet 625 nickel alloy and pure copper are shown in Fig. 2. The areas of the heat-resistant Udimet 625 nickel alloy and pure copper have no non-fusion in the joint zone.

However, macro defects were formed in the material of the vertical wall of the nozzle of the first type (Fig. 2*a*). This was due to the combination of the thicker steel substrate and high copper thermal conductivity that changed the heat transfer conditions. Porosity resulted from high temperature gradients and rapid solidification during nozzle fabrication due to non-optimized process parameters. The high electron beam power increased the heat input and therefore the temperature at which pore-like defects develop in the samples of the first type. In particular, the porosity is observed when depositing two rows of copper layers with a mean pore size of 75 μm. In addition, there are non-melts and voids with a mean size of 2.75 mm. The volume fraction of defects for samples of the first type did not exceed

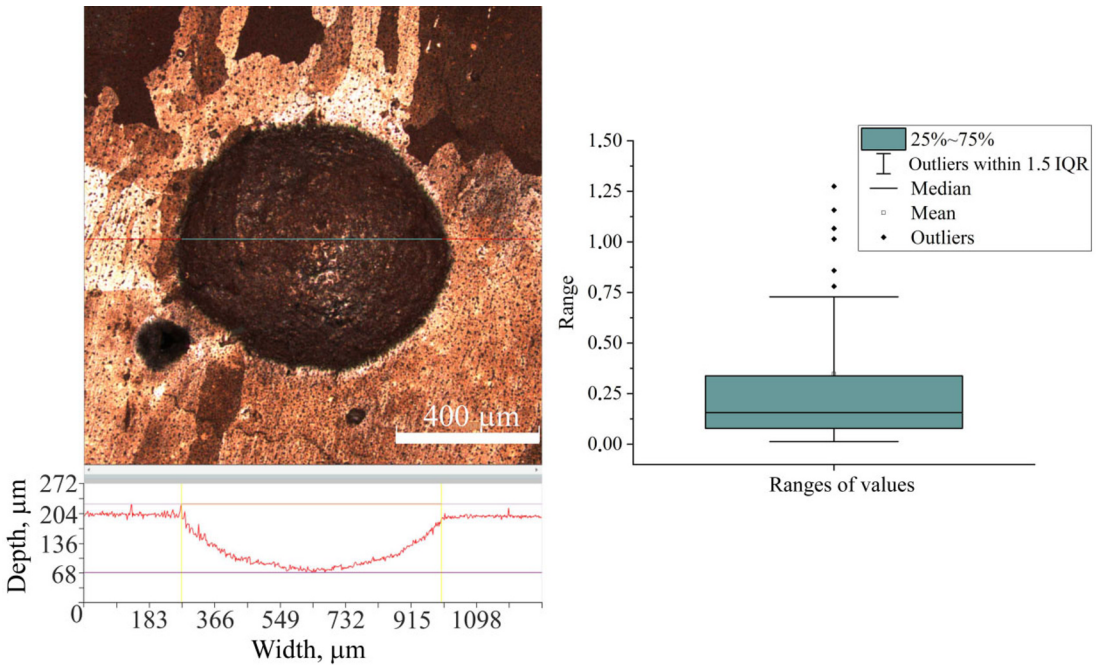

Fig. 3. Analysis of the porosity in the sample of the first type and block diagrams of pore measurements in the boundary zone without jumps in values beyond the error limits.

11%. Such rapid solidification contributed to a simultaneous increase in the porosity and microstructure refinement (Fig. 2*a*). Thus, the fine-grained structure (with a mean grain size of 20 μm) was formed on the first layers of the sample printed by the first type due to primary recrystallization. Since the additive method is characterized by high fabrication speed and low mobility of small-angle interfaces, the change in the volume fraction of interfaces is associated with the high temperature. Due to the large difference in the range of disorientation angles and axes of recrystallized grains, the mobility of boundaries increased. This led to an increase in the mean grain size up to 52 μm in the next layer. At a distance of 55 mm from the substrate, large free-form grains were observed with a size of 3.5 mm (Fig. 3*a*). The large grain can be formed from two neighboring seeds in the process of their coalescence and gradual growth.

In the course of growing of the sample of the second type, the defect-free surface was formed (Fig. 2*b*). In this case, the rapid heat dissipation by copper was compensated by using the thinner substrate. This confirms again the fact of pore formation in the material due to the non-optimized parameters in the first printing strategy. The first layers show a fine-grained structure similar to that of the samples of the first type. The next layer shows a change in the direction of grain growth. The deviation of the grain structure is due to the deviation in the direction of the temperature gradient during crystallization. In general, the elongated grains grow from the edge toward the center of the melt pool during solidification depending on their location. In this case, the heat flow direction depends largely on the local position at the melt boundary [9, 10]. At a distance of 15 mm from the substrate, the result of secondary recrystallization is observed, namely, the formation of oriented elongated grains the mean size of which is twice as large as that of the grains at a distance of 55 mm from the substrate in samples of the first type.

As already discussed above, the heat transfer conditions play an important role in the product formation. In the absence of thermal stability, the additive manufacturing of the products from dissimilar materials is characterized by a curved interface between the first deposited layer and the already solidified material [11]. This is due to sharp thermal gradients caused by different thermal conductivities of the materials. When the top layer is deposited, it is confined by the much colder bottom layer, causing elastic compressive deformation. At higher temperatures, however, the yield strength of the top layer decreases thereby allowing plastic compressive deformation. Cooling of the now plastically compressed top layer causes it to shrink thereby inducing a bending angle with respect to the direction of layer

TABLE 2. Chemical Composition of the Mechanical Mixture Region at the Boundary with the Inconel 625 Alloy, wt.%

	Cr	Ni	Cu	Mo	Zn	Nb	Fe	Ti
First type	4.8 ± 0.1	12.9 ± 0.1	78.9 ± 0.3	2.1 ± 0.1	0.1 ± 0.1	1.0 ± 0.1	0.1 ± 0.1	0.5 ± 0.1
Second type	8.1 ± 0.1	21.4 ± 0.1	64.1 ± 0.2	4.1 ± 0.1	0.4 ± 0.1	1.7 ± 0.1	0.1 ± 0.1	0.1 ± 0.1

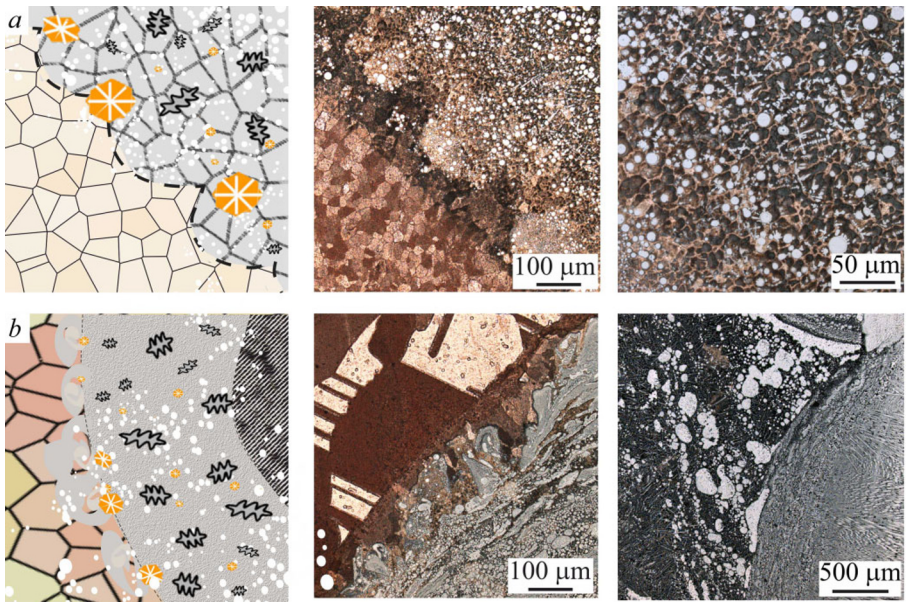

Fig. 4. Schematic and metallography images of the samples of the first (*a*) and second types (*b*) based on Inconel 625 and pure copper.

deposition. This results in tensile stress in the direction of growth. Thus, in the cross section of the experimental specimens of the first type, the penetration depth and the extent of the boundary vary chaotically. The presence of pore-like defects in the copper portion of the sample reduces the free surface energy, which initiates a change in the shape of the melt pool [1]. The instability of heat transfer and the high rate of heat dissipation together with different melting temperatures and densities of the employed materials cause the anisotropy of crystallization rate, leading to melting and re-solidification of copper. This, in turn, can inhibit the growth of the dendrite axes of the deposited nickel alloy. As the operating temperature during 3D printing increases, copper melts, while the nickel matrix remains the solid solution. At the same time, stirring occurs in the liquid state. Thus, in the samples of the first type, a fine dendritic structure and small rounded nickel alloy inclusions are formed in the copper matrix near the boundary during solidification (Fig. 4*a*). In the samples of the second type, the interface between the dissimilar materials is stable with the height of the whole sample. Due to the convective process in the melt pool, the primary residual droplet fraction is formed during the deposition of the nickel alloy, between which the fine-grained copper structure is located (Fig. 4*b*). In the specimens of the first type, the area of mechanical mixture near the curved interface is at l_2 = 1.15 mm.

The first deposited nickel alloy layer forms a roll on the surface [11]. The primary residual droplet fraction of the nickel alloy with an average size of 65 μm is formed together with the spherical inclusions of the nickel alloy up to 20 μm. The deposition of the next layer of the nickel alloy causes partial melting of the previous nickel layer and pulling of the copper alloy into this area due to surface tension (Fig. 4*b*). In the specimens of the second type, the area of mechanical mixture with different structural phase elements is at l_2 = 1.85 mm. Our analysis of the sample structure in the mechanical mixture region is fully correlated with the change in elemental composition (Table 2), where the composition of the nickel alloy in the as-deposited state differs from the initial wire composition (Table 1) by the higher copper content.

TABLE 3. Mechanical Test Characteristics of the Specimens of the Second Type

	σ_{YS}, MPa	σ_{US}, MPa	ε, %
Copper	49	215	25.4
Boundary zone	269	430	6.1
Boundary zone	305	389	3.7
Inconel 625	743	868	4.2

Moving from the interface toward the nickel alloy region, a dendritic structure is formed according to Hunt's crystallization theory [12]. In addition, the structure develops based on primary crystallization of austenite dendrites with subsequent solidification of copper between the arms of the first-order dendrites (Fig. 6*b*). When the next layer is deposited, the nickel alloy exhibits grain-dendrite morphology (Fig. 6*c*). This morphology includes both equiaxed and columnar grains. In the subsequent layers, down to the last layer, the structure is columnar dendritic. The dendrites are characterized by the first and second order arms with the second order poorly developed dendritic axes (Fig. 2*b*).

It is well known [13] that alloys with low thermal conductivity and high thermal expansion are more prone to cracking during the printing process. Two common types of cracking are layer solidification cracking and grain boundary cracking [14]. In the present work, the crack nucleation process during solidification of layers was recorded (Fig. 2*b*). It should be noted that the formation and propagation of cracks was stopped by the peculiarity of the additive technology – thermocycling.

The features of the microstructure identified above influence the mechanical properties of the specimrns. The tensile tests were carried out only on specimens of the second type. This is due to the fact that many defects, such as pores and non-melting, were found in the samples printed by the first type. The presence of defects is a sign of a low-quality product, as it negatively affects the result of the mechanical test. As can be seen, the test result near the substrate has worse strength characteristics (Table 3). This is due to the fact that the area of the working part of the specimen was more trapped in the copper area during cutting. The tensile specimens cut from the center and top of the test nozzle have similar characteristics, with tensile strengths σ_{US} = (410 ± 23) MPa, yield strength σ_{YS} = (287 ± 15) MPa, and elongation before fracture ε = (4.9 ± 0.7). With increasing distance from the interface, the material exhibited mechanical properties close to those of raw Incone l625 [15].

CONCLUSIONS

In this work, the surface morphology of the obtained products has been studied. It was found that on the outer surface of the samples of different types, the grain boundaries were well identified, and the grains were oriented at different angles relative to the substrate. Such peculiarity of the structure is explained by the influence of heat dissipation, the difference of which was provided by different thickness of the substrates. The grain sizes of the samples of two types differed significantly. In addition, in the sample of the first type, the pores seemed to be larger due to insufficient heating of the material during printing, and the grains were finer. Considering the quality of the formed layers of heterogeneous materials in the sample, it was found that 3D printing of the first type produced a high-amplitude *wave* within a single layer of the material. This is explained by the suboptimal temperature regime and, as a consequence, different crystallization times of the material during the manufacturing process, which leads to different thickness in different parts of the experimental sample. The higher values of the linear energy provided the most favorable structure. At the joint of dissimilar materials of pure copper and Inconel 625 nickel alloy, a clear interface was formed without visible defects such as pores, cracks, and voids. A curvilinear boundary zone was observed in which the formation of different structural phase components occurred, including solid solutions and mechanical mixtures. Thus, it has been shown that both geometric and electron beam parameters have a significant influence on the accuracy and quality of the products obtained by the wire electron beam additive method.

COMPLIANCE WITH ETHICAL STANDARDS

Author contributions

Conceptualization: A.V.C., V.E.R., E.A.K., and V.M.S.; investigation: Y.V.K.and K.S.O.; methodology: A.V.C.; original draft preparation K.S.O. and Y.V.K.; review and editing: A.V.C. and E.A.K. All authors have read and agreed to the published version of the manuscript.

Conflicts of interest

The authors declare that they have no known competing financial interests or personal relationships that could have appeared to influence the work reported in this paper.

Funding

The investigation was supported by the Russian Science Foundation (Grant No. 22-19-00578).

Financial interests

The authors have no relevant financial or non-financial interests to disclose.

Institutional review board statement

Applicable.

REFERENCES

1. E. A. Kolubaev, V. E. Rubtsov, A. V. Chumaevsky, and E. G. Astafurova, Phys. Mesomech., **25**, 479–491 (2022); DOI: 10.1134/S1029959922060017.
2. E. Akca and A. Gürsel, Period. Eng. Nat. Sci., **3**, 15–27 (2015); DOI: 10.21533/PEN.V3I1.43.
3. M. Perrut, P. Caron, M. Thomas, and A. Couret, C. R. Phys., **19**, 657–671 (2018); DOI: 10.1016/J.CRHY. 2018.10.002.
4. F. Wang, D. Ma, and A. Bührig-Polaczek, Mater. Charact., **127**, 311–316 (2017).
5. T. J. Horn and D. Gamzina, in: Additive Manufacturing Process, V. 24, D. L. Bourell, W. Frazier, H. Kuhn, and M. Seifi, eds., ASM International (2020), pp. 388–418; DOI: 10.31399/ASM.HB.V24.A0006579.
6. C. Zeng, H. Wen, B. C. Bernard, *et al*., Manuf. Lett., **28**, 25–29 (2021); DOI: 10.1016/J.MFGLET. 2021.02.002.
7. H. C. DeGroh, D. L. Ellis, and W. S. Loewenthal, J. Mater. Eng. Perform., **17**, 594–606 (2008); DOI: 10.1007/ S11665-007-9175-3.
8. S. Moriya, T. Inoue, M. Sasaki, *et al*., Trans. JPN Soc. Aeronaut. Space Sci., **16**, 261–266 (2018); DOI:10.2322/TASTJ.16.261.

9. A. A. Antonysamy, J. Meyer, and P. B. Prangnell, Mater. Charact., **84**, 153–168 (2013); DOI: 10.1016/j.matchar.2013.07.012.
10. H. Zhao and T. Debroy, Metall. Mater. Trans. B, **32**, 163–172 (2001); DOI: 10.1007/s11663-001-0018-6.
11. H. Inoue, T. Koseki, S. Ohkita, and M. Fuji, Sci. Technol. Weld. Join., **5**, 385–396 (2000); DOI: 10.1179/136217100101538452.
12. J. Yin, L. L. Yang, X. Yang, *et al*., Addit. Manuf., **29**, 200778 (2019); DOI: 10.1016/j.addma.2019.100778.
13. K. Puebla, L. E. Murr, S. M. Gaytan, *et al*., Mater. Sci. Appl., **3**, 259–264 (2012); DOI: 10.4236/msa. 2012.35038.
14. K. Kalashnikov, T. Kalashnikova, V. Semenchuk, *et al*., Metals, **12**, 2048 (2022); DOI: 10.3390/met12122048.